Clays and Clay Minerals, Vol. 49, No. 6, 596–607, 2001.

KAOLINITE TO HALLOYSITE-7 Å TRANSFORMATION IN THE KAOLIN DEPOSIT OF SÃO VICENTE DE PEREIRA, PORTUGAL

IULIU BOBOS[1], JOELLE DUPLAY[2], JOÃO ROCHA[3] AND CELSO GOMES[1]

[1] Department of Geosciences, University of Aveiro, 3810-Aveiro, Portugal
[2] Centre de Geochémie de la Surface, Universite "Louis Pasteur", 67084-Strasbourg Cedex, France
[3] Department of Chemistry, University of Aveiro, 3810-Aveiro, Portugal

Abstract—The transformation of kaolinite to halloysite-7 Å was identified in the kaolin deposit of São Vicente de Pereira (SVP), using X-ray diffraction (XRD), Fourier transform infrared spectroscopy (FTIR) and transmission electron microscopy (TEM). Both the $02,1\bar{1}$ and $1\bar{3},13$ reflections show changes in the XRD patterns along the kaolinite to halloysite-7 Å transition, and the FTIR spectra show changes corresponding to both OH^- and Si–O–stretching bands and Al–O–Si–bending vibrations. The interlayer water content in the kaolinite structure increases during transition. The two-layer periodicity of well-ordered kaolinite and rolling up of kaolinite plates are observed using high-resolution transmission electron microscopy (HRTEM). Long and short tubes exhibit halloysite-7 Å. No structural Fe was found in the kaolinite samples. Analytical electron microscopy (AEM) indicates no substitution of Al^{3+} for Si^{4+}. The Si/Al ratio shows values of ~1 for the kaolinite and rolled kaolinite plates. The ^{27}Al magic angle spinning neutron magnetic resonance (MAS-NMR) spectra display a resonance centered at ~1 ppm, assigned to six-coordinated aluminum. The transformation of kaolinite to halloysite-7 Å is controlled by surface reaction.

Key Words—Kaolinite to Halloysite-7 Å Transformation, Hydration, Rolling and Folding, Surface Reaction Control, Portugal.

INTRODUCTION

Kaolinite, one of the most abundant clay minerals, occurs widely in soils, sediments and altered rocks. It may form from feldspars and/or micas by weathering or hydrothermal processes or it may crystallize direct from solution (Stoch and Sikora, 1976; Keller, 1978; Wilke *et al.*, 1978; Meunier and Velde, 1979; Anand *et al.*, 1985; Banfield and Eggleton, 1990; Robertson and Eggleton, 1991; Jiang and Peacor, 1991; Singh and Gilkes, 1992). Topotactic or epitactic alteration of mica or feldspar to halloysite has not previously been identified in nature (Gilkes *et al.*, 1986; Singh and Gilkes, 1992), whereas kaolinite formed from mica by topotactic alteration can subsequently produce halloysite tubes (Giese, 1988). Nevertheless, halloysite may also be formed through alteration of feldspar via solution or a non-crystalline intermediate stage (Eswaran and Bin, 1978; Singh and Gilkes, 1992).

Robertson and Eggleton (1991) explained the transformation of platy kaolinite into spiral halloysite rods by a loss of structural rigidity at points along the kaolinite crystal due to hydration of kaolinite. Also, Singh and Gilkes (1992) showed a development of parallel halloysite tubes and laths through deformation of platy kaolinite pseudomorphs after mica. These authors described the tranformation of kaolinite plates by fragmentation into laths that rolled or folded to form halloysite tubes.

Using kaolinite from Georgia (USA), Singh and Mackinnon (1996) tested the hypothesis that platy kaolinite will roll upon hydration. The HRTEM images of cross-sections of tubes formed after repeated cycles of kaolinite hydration showed both curved layers and planar faces, supporting their hypothesis.

By contrast, the reverse transformation of halloysite-7 Å to kaolinite was recognized by Churchman and Gilkes (1989) in the lateritic profiles of dolerite and granite.

A gradual transition from well-ordered to poorly-ordered kaolinite was found along a geological profile in the kaolin deposit of SVP from Portugal. The present contribution reports the transformation of kaolinite to halloysite-7 Å and structural, morphological and crystallochemical results are discussed.

GEOLOGICAL SETTING

The kaolin deposit of SVP is situated at the northwestern edge of the Ossa Morena zone (OM-Z) and extends along a NNW–SSE transect that separates the two lithostratigrafic units of Lourosa and Arada (Figure 1).

The migmatite and/or migmatite gneiss are argillic, altered due to either hydrothermal or supergene processes. Bobos and Gomes (1998) described a greisen alteration (quartz + muscovite bearing F, Cl and quartz + tourmaline assemblages) and an argillic alteration (including post-greisen type alteration) represented by well-ordered kaolinite ± illite assemblage. Tourmaline ± quartz veins cross-cut the argillized migmatite rocks (rich in kaolinite). Weathering is characterized by hydration of well-ordered kaolinite that led to the transformation of kaolinite into halloysite-7 Å. However,

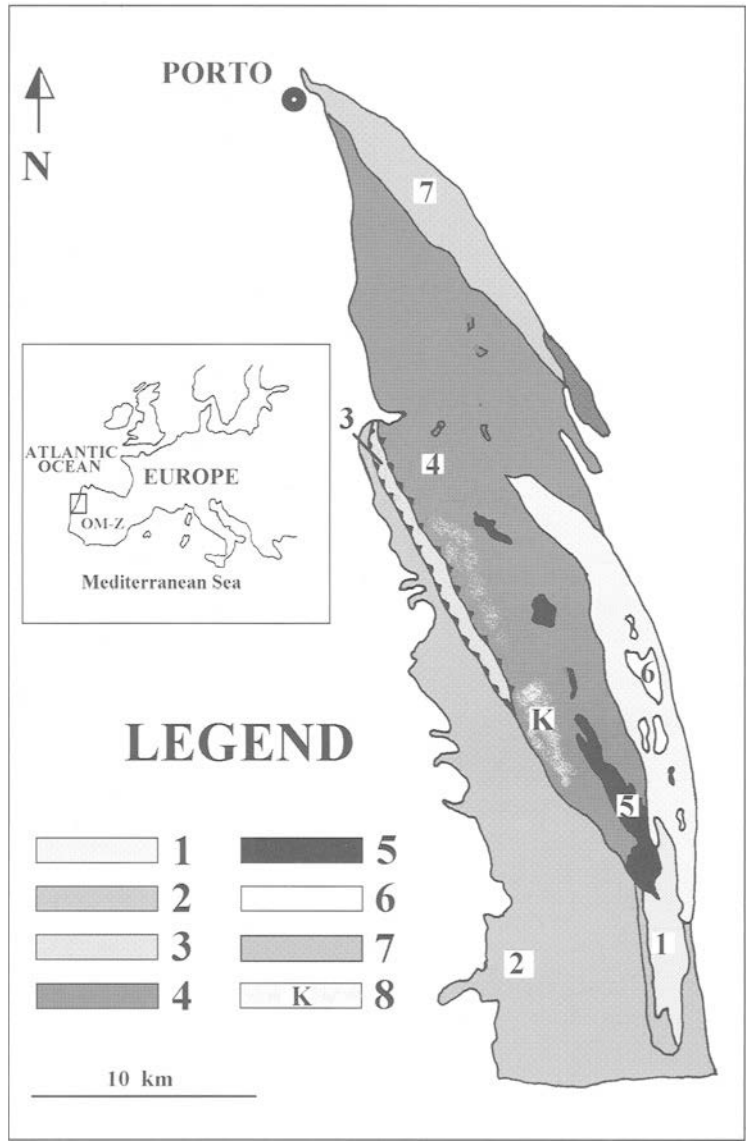

Figure 1. Location and geological map of the northwestern sector of the Ossa-Morena zone (after Chaminé *et al.*, 1995). 1—São João de Ver Unit (metavolcanite, metaporphyry, micaceous schist, metagraywacke); 2—Arada Unit (green schist, amphibolite schist, quartzite with garnet); 3—Espinho Unit (staurolite + micaceous schist, quartzite with garnet); 4—Lourosa Unit (micaceous schist, orthogneiss, migmatite, amphibolite); 5—Hercynian granitoids (syn D3); 6—Ante-Hercynian granitoids; 7—Post-tectonic granitoids (granitoids of Madalena); 8—Localization of the São Vicente de Pereira kaolin deposit (K).

another generation of halloysite-7 Å identified in the kaolin deposit of SVP, was formed from K-feldspar dissolution via a Si-Al gel (Bobos and Gomes, 2000). No other products typical of weathering were identified.

Hydrothermal activity in the kaolin deposit of SVP was related to metamorphic fluids (Bobos and Gomes, 1999) associated with a deformational system which includes faults, fractures and dilatation zones known as "ductile shear zones" (Ribeiro *et al.*, 1980).

In the north sector of the kaolin deposit, a cross-section with E–W trend was studied, where transition from well-ordered kaolinite to halloysite-7 Å, via poorly-ordered kaolinite was identified. The samples were collected from the central part of kaolin deposit to the diffuse contact between the argillic altered migmatite complex and micaschist complex.

MATERIALS AND METHODS

Terminology

The terms 'transition' and 'transformation' used in this paper refer to two distinct processes, *i.e.* transition implies a structural passage from ordered to disordered

https://doi.org/10.1346/CCMN.2001.0490609 Published online by Cambridge University Press

structure observed by XRD and FTIR techniques, whereas transformation refers to a morphological feature expressed by a topotactic transformation of kaolinite to halloysite-7 Å.

The Hinckley index (HI) was calculated in order to assess the kaolinite crystallinity (Hinckley, 1963). We interpreted the HI in accordance with the method suggested by Plançon *et al.* (1988) and by Plançon and Zacharie (1990) which shows that HI is an empirical calculation and is not based entirely on the crystalline structure of kaolinite.

Preparation of materials

The HI was measured for 30 specimens of kaolinite (<2 μm clay-aggregate fractions) and three main groups were established: high crystallinity (HI >0.9), medium crystallinity (HI = 0.5–0.9) and low crystallinity (HI <0.5). Only three samples (SVP-7, SVP-44 and Hly-8) were selected from each group.

Either <10 μm or <2 μm clay-aggregate fractions were separated from aqueous suspensions by the sedimentation method (Stokes' law). The <2 μm clay fraction was washed and concentrated by centrifugation and then air dried at 40°C overnight to avoid possible collapse of halloysite-10 Å to halloysite-7 Å. A chemical treatment (Jackson, 1975) was used to remove a Si-Al gel identified in the kaolinite samples.

Prior to particle-size analysis, Na hexametaphosphate followed by ultrasonic treatment were used to obtain good particle dispersion.

The structural behaviour of kaolinite was tested using organic molecule intercalation. Oriented kaolinite specimens were prepared on glass slides; afterwards organic molecules (dimethylsulfoxide and K acetate) were intercalated in a saturated environment at 60°C for 48 h. The hydrazine test was used to identify mixtures of kaolinite and halloysite-7 Å (Range *et al.*, 1969).

Disc-shaped samples were obtained by pressing a mixture of 1 mg sample with 200 mg of KBr. The disc-shaped samples were heated at 150°C prior to FTIR analysis, in order to remove the hydration water.

The <2 μm clay-aggregate specimens were dispersed using an ultrasonic bath and after a convenient dilution, one drop of the suspension was deposited on a copper microgrid, previously covered with a formvar film. Before HRTEM analysis, the <2 μm kaolinite suspensions were oriented in a plastic tray support, dried at 40°C, and embedded in Spurr's resin. Ultrathin sections were cut with a diamond knife at 50 μm thick using a Reichert microtome.

Methods

Particle size. The particle-size distribution of the <2 μm clay-aggregate specimens was determined using a Sedigraph (Micromeritics 5100) in the range 10–0.2 μm. The pH was measured using a pH meter apparatus (Corning 240, UK) calibrated with buffer solutions (pH 7 and 10 Merck, Germany).

X-ray diffraction. The specimens were prepared as randomly oriented clay-aggregate specimens for XRD analysis using a Rigaku Geigerflex D/max.–C series diffractometer equipped with CuKα radiation and a graphite monochromator. A step size of 0.02°2θ and 10 s counting time for randomly oriented aggregate specimens and 5 s for oriented clay-aggregate specimens were used. The *d*(*hkl*)-spacings and reflection intensities were measured using a computer program (IBM PC—software for DMAXB Controller).

Fourier transform infrared spectroscopy. The FTIR spectroscopy (transmittance mode) was performed using a Mattson-7000 apparatus in the frequency range 4000–400 cm^{-1}, equipped with a DTGS (deuterated triglycine sulfate) single plate detector.

Transmission electron microscopy. The microscopic observations were performed using an Hitachi H9000-NA transmission electron microscope, working at 300 kV, equipped with a solid-state quantum detector (Kevex, USA) for X-ray energy dispersive spectroscopy (EDS). Selected area electron diffraction (SAED) was used to determine the crystalline or amorphous character of the minerals, using apertures of 5–50 μm to select 0.1–1.5 μm areas. A gold standard was used for SAED pattern calibration. The HRTEM was performed using a Philips CM12 electron microscope (at "Louis Pasteur" University of Strasbourg, France).

Analytical electron microscopy. This method was used for chemical analysis of kaolinite crystals. The chemical data reported are the average of *n* analyses performed on the same types of crystal. A conventional *k* factor was used according to various chemical compositions determined previously (Ma *et al.*, 1998).

The ^{27}Al-magic angle spinning neutron magnetic resonance. The ^{27}Al-MAS-NMR spectra were recorded at 104.3 MHz on a (9.4 T) Bruker MSL 400P spectrometer using short, powerful radio-frequency pulses (0.6 μs equivalent to 10° pulse angle), a spinning rate of 14 kHz and a recycle delay of 1 s. To remove the strong ^{1}H-^{27}Al dipolar interaction, high-power (B_1 field amplitude ~70 kHz) ^{1}H decoupling was used. Chemical shifts are quoted in ppm from $[Al(H_2O)_6]^{3+}$.

RESULTS

X-ray diffraction

Randomly oriented clay-aggregate analyses. Three selected kaolinite samples analyzed using XRD (Figure 2) show the structural transition from well-ordered kaolinite (HI = 1.07) to halloysite-7 Å, via poorly-ordered kaolinite HI = 0.56). Structurally well-ordered kaolinite (SVP 7) is characterized by well-resolved 02,1$\bar{1}$ and 1$\bar{3}$,13 reflections (Figure 2a). The 02,1$\bar{1}$ re-

https://doi.org/10.1346/CCMN.2001.0490609 Published online by Cambridge University Press

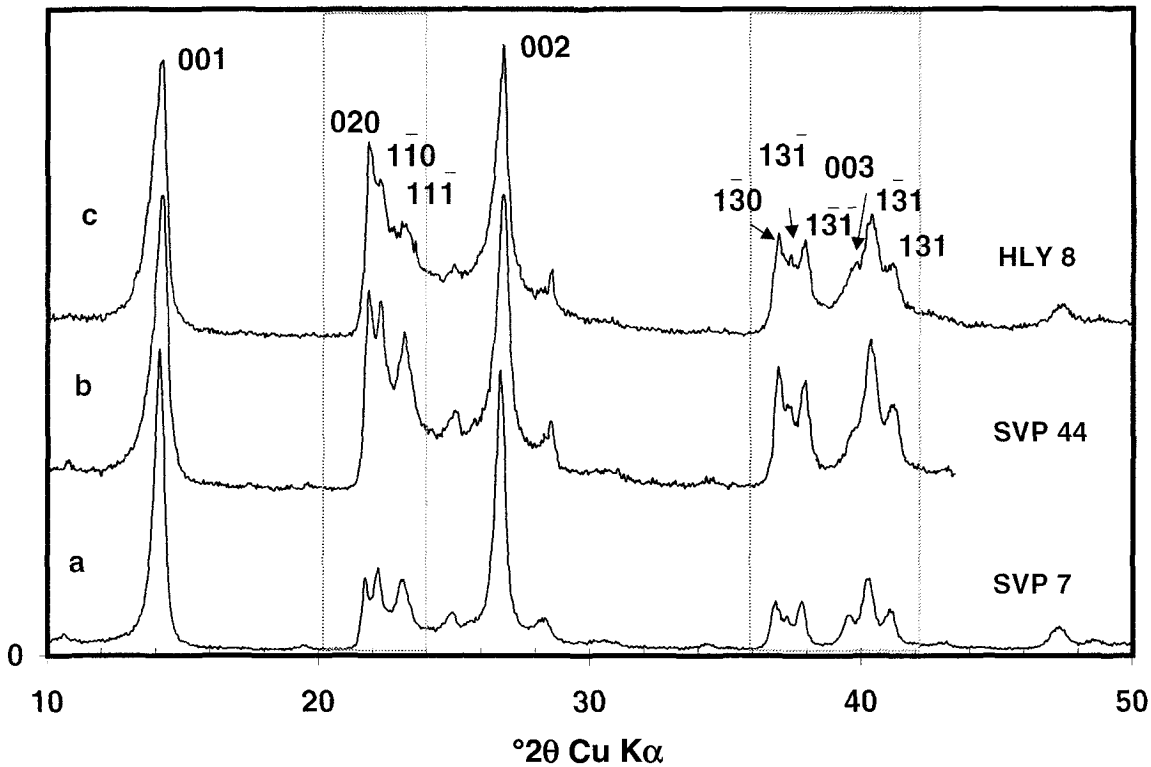

Figure 2. XRD patterns of well-ordered kaolinite (a), poorly-ordered kaolinite (b) and halloysite-7 Å (c).

flections show changes both in intensity and resolution during transition. The intensity of the $1\bar{1}0$ and $11\bar{1}$ reflections corresponding to well-ordered kaolinite, were compared with the intensity of the 020 reflection, the latter being progressively shorter than the former. In comparative terms, the 020 reflection increases in intensity during transition, whereas both $1\bar{1}0$ and $11\bar{1}$ reflections decrease in intensity, changing to weakly modulated reflections (Figure 2b, c).

Changes both in intensity and resolution of the $1\bar{3},13$ reflections in the range 36–42°2θ took place during the kaolinite to halloysite-7 Å transition. The X-ray pattern of well-ordered kaolinite shows two clearly resolved reflection triplets in the range 36–42°2θ. Both the $1\bar{3}0$ and $13\bar{1}$ reflections are well-resolved either in well-ordered kaolinite or poorly-ordered kaolinite, indicating its triclinic character (Plançon and Tchoubar, 1977). Whenever kaolinite structural order decreases, the intensity of the $1\bar{3}0$ reflection increases. Within the range 39–42°2θ, the triplet 003, $1\bar{3}1$ and 131 reflections observed in well-ordered kaolinite (Figure 2a) transforms into a doublet in poorly-ordered kaolinite and halloysite-7 Å (Figure 2b). The intensity of the 003 reflection transforms into a shoulder at the $1\bar{3}1$ reflection.

The intensities of both the 001 and 002 reflections decrease as the order decreases. Also, the shape of the 001 reflection became more asymmetric as the disorder decreased.

Dimethylsulfoxide, K acetate and hydrazine intercalation. Dimethylsulfoxide (DMSO) was intercalated in the kaolinite structure and then the complex was XRD analysed. After intercalation, the 7.2 Å peak shifted to 11.2 Å. A residual 7.2 Å peak remained visible, because DMSO did not completely intercalate in the kaolinite structure. The 7 Å residual peak was almost absent in poorly-ordered kaolinite.

X-ray patterns of K acetate intercalated in well-ordered kaolinite and poorly-ordered kaolinite showed a very sharp peak at 14.10 Å. Also, a residual peak at 7.2 Å occurred. After 15 washing cycles, K acetate had been partially removed and the two peaks were still present at 7.9 Å and 7.2 Å. The intensity of the 7.2 Å peak increased after the organic molecules were removed.

After hydrazine intercalation, the 7 Å peak expanded to 10 Å and became broader. Nevertheless, the 7 Å residual peak appeared in both well-ordered kaolinite and poorly-ordered kaolinite. The 10 Å peak collapsed at 7.2 Å after hydrazine was removed and an intermediate reflection at 8.42 Å appeared. After 10 washing cycles the 8.42 Å peak collapsed at 8.20 Å. After 35 cycles the intermediate reflection disappeared com-

https://doi.org/10.1346/CCMN.2001.0490609 Published online by Cambridge University Press

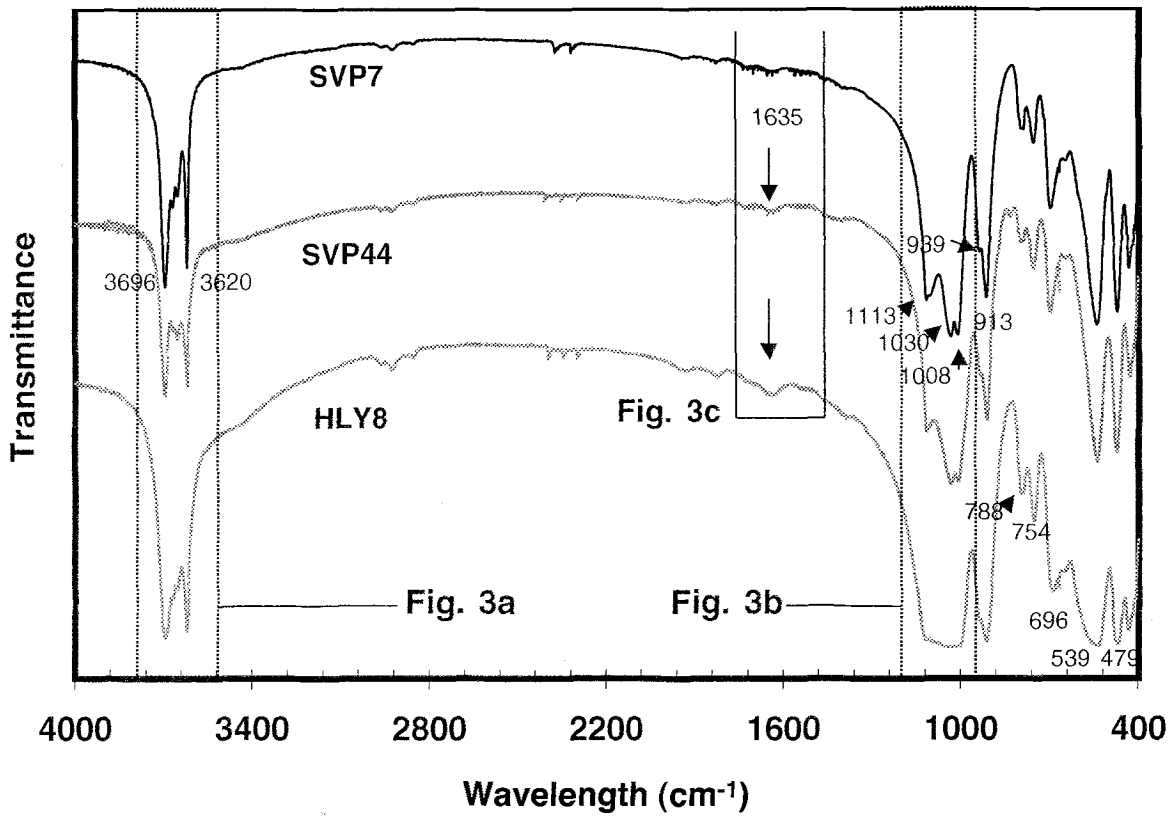

Figure 3. FTIR spectra of well-ordered kaolinite, poorly-ordered kaolinite and halloysite-7 Å. (a) Selected OH^--stretching bands in the range 3700–3500 cm^{-1}. (b) Selected Si–O-stretching bands in the range 1200–950 cm^{-1}. (C) Selected H–O–H bands at 1630 cm^{-1}.

pletely. The intensity of the 7.2 Å peak increased after each washing cycle. The position of the intermediate reflection depends on the degree of organic molecule intercalation. The mixture of kaolinite and halloysite-7 Å was only identified in the Hly-8 sample, where the 10 Å peak remained after hydrazine removal. In quantitative terms, the kaolinite:halloysite ratio was estimated as 1:6.

Fourier transform infrared spectroscopy

The OH-stretching region of well-ordered kaolinite is characterized by four bands essentially unchanged at 3694, 3668, 3526 and 3620 cm^{-1}, whereas poorly-ordered kaolinite displays only three bands (Figure 3a). The FTIR spectrum of halloysite-7 Å is characterized by two OH-stretching bands at 3696 and 3620 cm^{-1} of lower intensity and broader; two small inflexions occur between them (Figure 3a).

The Si–O stretching region comprises three absorption bands at 1114, 1030 and 1008 cm^{-1} either in well-ordered or poorly-ordered kaolinite (Figure 3b). In sample Hly-8 the Si–O stretching exhibits a broader range. The doublet from 1030 and 1008 cm^{-1} disappears and becomes broader. However, a small peak at 1114 cm^{-1} may be seen (Figure 3b).

The Al–OH bond at 939 cm^{-1} assigned to the inner OH^- surface, occurs as a small inflexion to the OH^--bending vibrations of inner hydroxyl groups at 913 cm^{-1} apparently sharp during transition, but is broader in sample Hly-8.

The stretching band Si–O at 696 cm^{-1} is sharp in the first two samples, whereas sample Hly-8 has lower intensity and is broader. The bands at 539 and 470 cm^{-1} assigned to the Al–O–Si and Si–O–Si bending vibrations are sharp in well-ordered kaolinite, whereas in the halloysite-7 Å sample they are broader.

The intensity of the H–O–H deformation band at 1635 cm^{-1} increases as the structural order decreases and as the interlayer water content increases, the intensity of the same band increases and broadens (Figure 3c).

Particle-size distribution

An analysis of the particle-size distribution was performed for aggregates and particles of kaolinite (Figure 4). The <10 μm clay aggregate fraction of well-ordered kaolinite (SVP-7) is concentrated in the range 2–0.6 μm, whereas the same fraction of poorly-ordered kaolinite (SVP 44) occurs in the range 2–1 μm.

https://doi.org/10.1346/CCMN.2001.0490609 Published online by Cambridge University Press

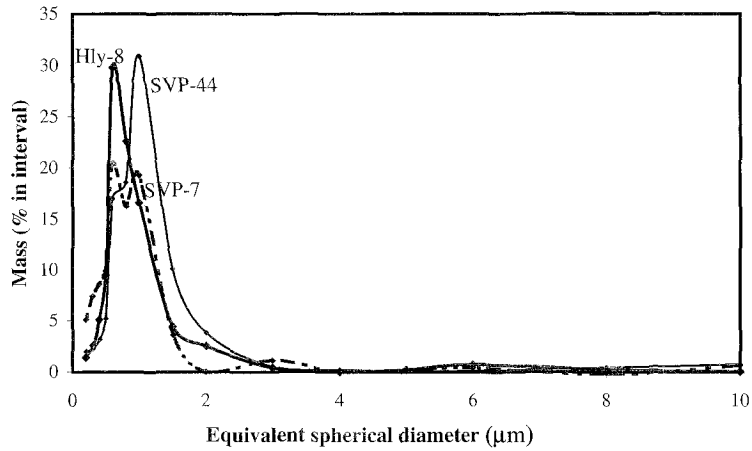

Figure 4. Particle-size distribution of kaolinite samples (SVP-7, SVP-44 and Hly-8).

The particle-size distribution of the Hly-8 sample has the equivalent spherical diameter in the range 1–0.8 μm.

Transmission electron microscopy

Several morphological features were observed: aggregates of kaolinite booklets, pseudohexagonal plates, thin irregular plates exhibiting both rolling-up on their surfaces and short tubular forms at their edges, partially rolled fragmented plates and well-defined long tubes.

Well-ordered kaolinite (SVP-7) contains aggregates of booklets. Kaolinite plates grew syntaxially and display aggregates of individual particles oriented along the **c*** direction (Bobos and Gomes, 1998). Poorly-ordered kaolinite exhibits individual pseudohexagonal kaolinite plates (Figure 5a). Two morphologies were recognized corresponding to sample Hly-8 (Figure 5b): long tubes elongated along the **a*** direction and short tubes elongated along the **b*** direction. Very thin pseudohexagonal plates of kaolinite showing rolling-up are identified in sample Hly-8 (Figure 6). Rolling-up preferentially follows one crystallographic direction. The SAED performed on kaolinite plates yields a hexagonal 'single spot', exhibiting a *hk*0 pattern (Figure 6). Transformation of kaolinite into halloysite-7 Å is suggested by rolling-up of kaolinite platy crystals into tubes.

The lath shape apparently interpretable as halloysite-7 Å aggregates corresponds to kaolinite (Figure 7a). The SAED carried out on single crystal gives an hexagonal reflection spot similar to that obtained for kaolinite (Figure 7b). The lath-shaped kaolinite crystals are folded or rolled. Halloysite exhibits an intermediate spherical shape formed from lath kaolinite rolled

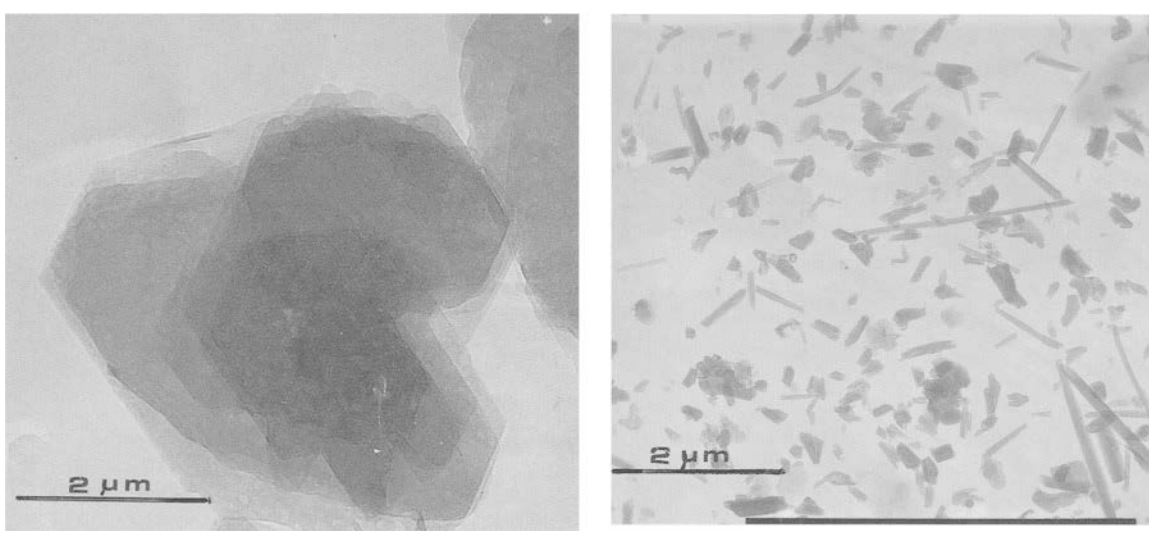

Figure 5. TEM images showing: (a) pseudohexagonal plates of poorly-ordered kaolinite; (b) long and short tubes of halloysite-7 Å and lath-shaped kaolinite plates rolled.

https://doi.org/10.1346/CCMN.2001.0490609 Published online by Cambridge University Press

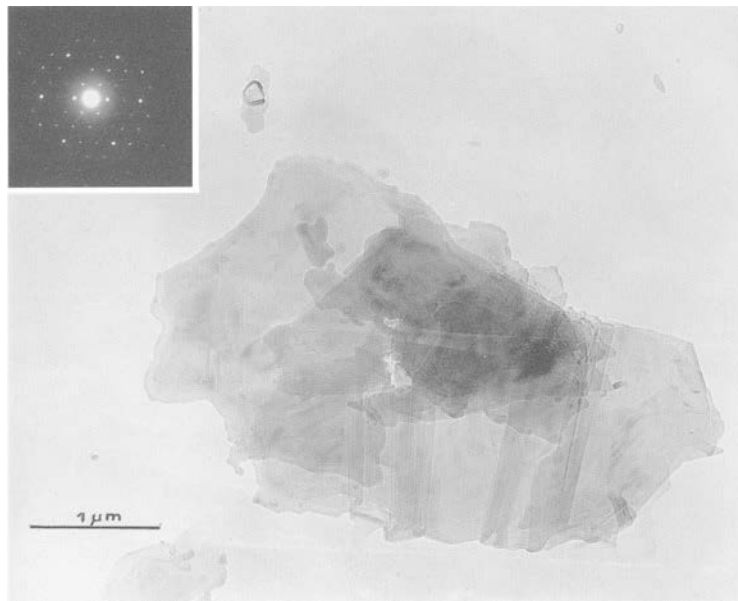

Figure 6. TEM image showing kaolinite plates rolling-up along the **b*** direction. SAED shows the *hk*0 pattern of the kaolinite structure.

(Figure 7c). The diameter estimated for a tube of halloysite is ~14 nm (Figure 7d). These results constitute the unique relationship between the two minerals.

A representative HRTEM image of well-ordered kaolinite (SVP-7) exhibits the 7 Å basal lattice fringes with a two-layer periodicity (Figure 8). Two sections were chosen: (1) the first section (a) shows the basal lattice fringes of 7 Å coherent layers; (2) the second section (b) reveals some defects (indicated by arrows), exhibiting deformation and terminated layers. Non-basal $0\bar{2}1$ fringes are crossing the basal 001 lattice fringes.

Analytical electron microscopy

Crystals of well-ordered kaolinite, poorly-ordered kaolinite and halloysite-7 Å were analyzed by AEM (Table 1). Structural Fe was not detected. The Si/Al ratio calculated on sets of well-ordered kaolinite to poorly-ordered kaolinite and rolled kaolinite plates (Figure 6) or folded lath kaolinite (Figure 7a) show values of ~1. Nevertheless, long tubes of halloysite-7 Å show a slightly smaller Si content and greater Al content.

^{27}Al-magic angle spinning neutron magnetic resonance

The ^{27}Al MAS-NMR spectra of the samples studied (Figure 9) display the second-order quadropole powder pattern centered at ~1 ppm, assigned to six-coordinated aluminum (Rocha and Klinowski, 1990; Rocha and Pedrosa de Jesus, 1994). The full-width-at half-maximum (FWHM) of this line increases from 9.4 ppm for well-ordered kaolinite to 10.00 ppm for halloysite, whereas for poorly-ordered kaolinite it is 10.8 ppm. The increasing FWHM of this resonance is due to a larger distribution of quadropole coupling parameters and isotropic chemical shifts brought by structural disorder that arises primarily as the result of Al-vacancy displacements in the octahedral sheet (Newman *et al.*, 1994). In addition to the six-coordinated aluminum peak, the spectrum of poorly-ordered kaolinite displays a resonance at ~70 ppm attributed to four-coordinated aluminum. This resonance accounts for ~9% of the total spectral intensity in the range 100–50 ppm. Well-ordered kaolinite also gives a very faint (intensity 1% or less) peak at ~70 ppm.

DISCUSSION

The powder XRD patterns show structural characteristics interpreted as variable order-disorder of kaolinite. The structural data observed serve as a basis for inferring the transition and transformation of kaolinite into halloysite-7 Å. The relationship between kaolinite and halloysite-7 Å should include trends of intermediate stages between the two separate mineral species (Churchman and Gilkes, 1989). The kaolinite to halloysite-7 Å transition is expressed by (1) decrease of the structural order, and (2) increase of the structural water content.

The organic molecules did not completely intercalate in the kaolinite samples studied. Reports of partial intercalation of organic molecules are known from the literature (MacEwan and Wilson, 1980). Random interstratification of 10 Å and 7.2 Å kaolinites during organic molecule intercalation was observed and discussed.

https://doi.org/10.1346/CCMN.2001.0490609 Published online by Cambridge University Press

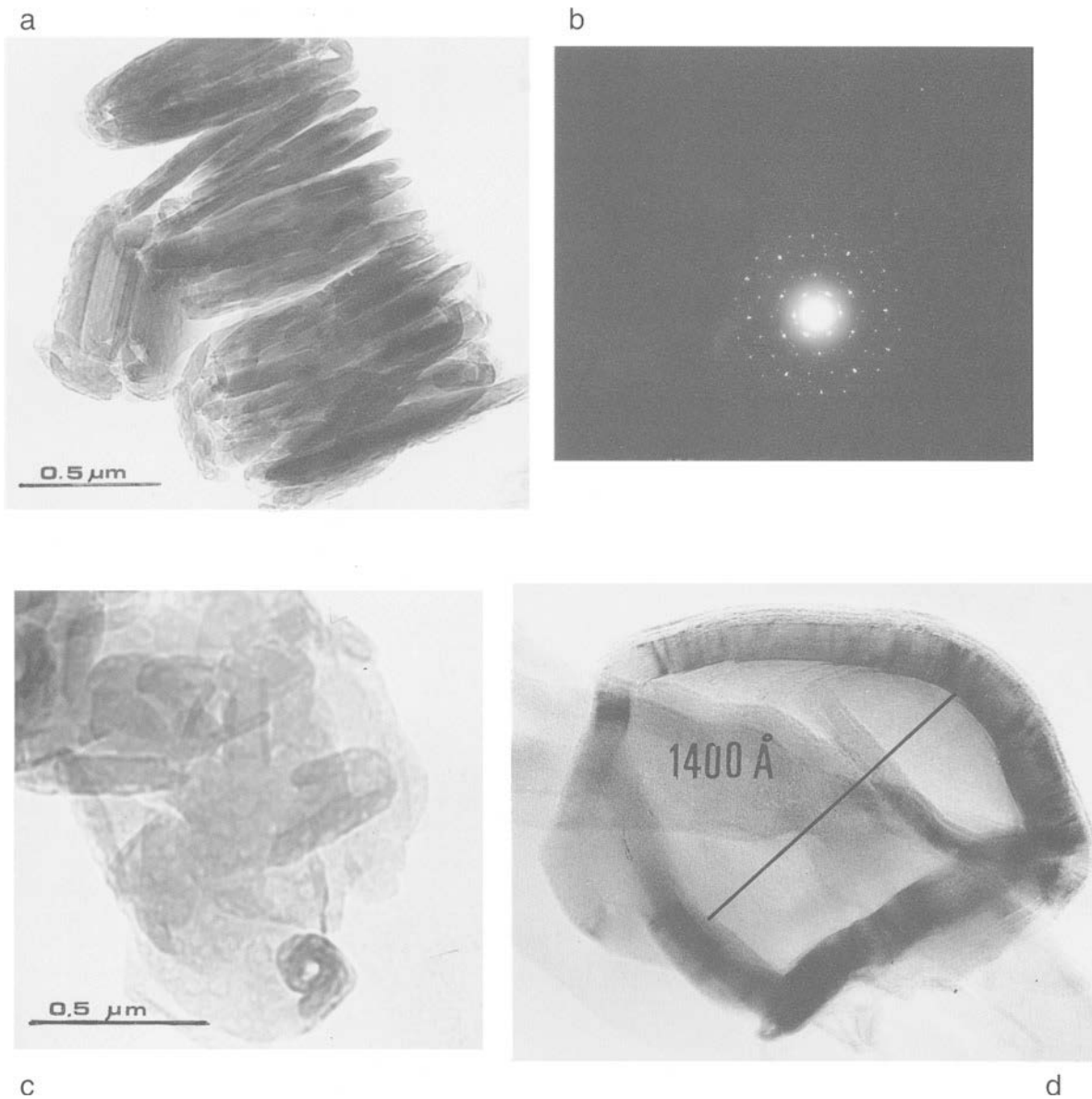

Figure 7. (a) Aggregates of folded lath-shaped kaolinite. (b) SAED pattern confirms the structure of kaolinite. (c) TEM image exhibiting rolled-up lath-shaped kaolinite. (d) HRTEM image of a section of a tube of halloysite-7 Å.

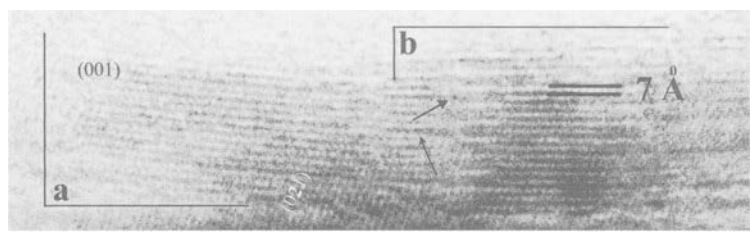

Figure 8. HRTEM image of well-ordered kaolinite. Some coherent 7 Å layers are observed in sector a and some defect layers (arrows) in sector b.

https://doi.org/10.1346/CCMN.2001.0490609 Published online by Cambridge University Press

Table 1. Chemistry of individual crystals of kaolinite and halloysite-7 Å.

Samples	SiO_2	Al_2O_3	SiO_2/Al_2O_3	Si	Al	Si/Al	δ	Morphology
	n = 6	n = 6						
SVP-7	53.76	46.24	1.16	1.99	2.01	0.99	0.1	pseudo-hexagonal crystal
SVP-7	53.91	46.08	1.17	1.99	2.01	0.99	0.1	pseudo-hexagonal crystal
SVP-44	53.61	46.39	1.15	1.98	2.02	0.98	0.1	pseudo-hexagonal crystal
Hly-8	53.71	46.29	1.16	1.99	2.01	0.99	0.1	kaolinite plates rolled
Hly-8	53.63	46.37	1.16	1.98	2.02	0.98	0.1	lath kaolinite
Hly-8	53.11	46.89	1.13	1.96	2.04	0.96	0.1	long tubes of halloysite

n = number of analysis; δ = standard deviation.

Particle-size distribution decreases along transition. This is due to exfoliation of booklets of kaolinite plates caused by hydration of kaolinite. The well-ordered kaolinite (SVP 7) displays a bi-modal distribution, whereas poorly-ordered kaolinite (SVP 44) exhibits a log-normal distribution. The halloysite-7 Å sample (Hly-8) has a smaller and narrower average particle-size distribution than the other two samples. The particle shape is reflected in their size-distribution curves.

Hydration is a chemical process related to weathering. Kaolinite hydration involves adsorption of water molecules on external and internal surfaces of particles and may form interlayer hydration complexes. As the degree of hydration increases, the disorder in the kaolinite structure increases (Wada, 1961; Costanzo *et al.*, 1984). The FTIR spectra show that hydration increases during the kaolinite to halloysite-7 Å transition, whereas XRD patterns show an increase of disorder in kaolinite.

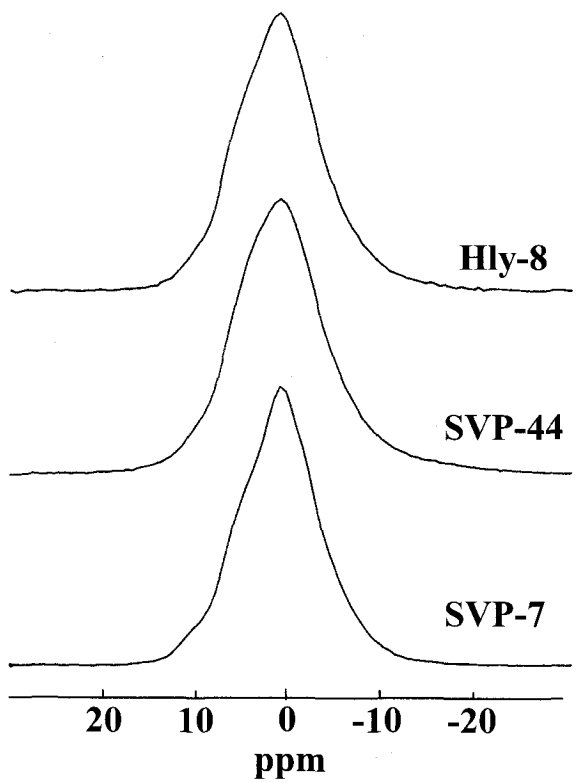

Figure 9. The ^{27}Al MAS-NMR spectra of (a) well-ordered kaolinite, (b) poorly-ordered kaolinite, and (c) halloysite-7 Å.

Individual pseudohexagonal plates of kaolinite were found in poorly-ordered kaolinite (SVP-44), whereas in well-ordered kaolinite, aggregates of kaolinite booklets occur. The Hly-8 sample is of lath-shaped kaolinite and halloysite-7 Å crystals formed from kaolinite or Si-Al gel. Long tubes of halloysite-7 Å are genetically related to a Si-Al gel which resulted from K-feldspar dissolution (Bobos and Gomes, 2000), whereas the short tubes were formed by folding/rolling of kaolinite plates. The XRD pattern of the Hly-8 sample displays a poorly-ordered kaolinite structure. A hydrazine test confirmed a mixture of kaolinite and halloysite-7 Å. Otherwise, the TEM image exhibits short and long tubes of halloysite-7 Å, curved/folded lath-shaped kaolinite plates and rolled kaolinite plates (Figure 6b). Short tubes elongated along the **b*** direction correspond to folded lath-shaped kaolinite. Rolled/folded fractured plates of kaolinite yielded an XRD pattern similar to that for a poorly-ordered kaolinite structure. The SAED pattern obtained on apparent halloysite tubes (Figure 7) confirm a pattern typical of kaolinite.

Honjo *et al.* (1954) and Kohyama *et al.* (1978) investigated halloysite crystals by SAED, identifying a structure based on two-layer periodicity, named "tubular kaolinite". Using electron diffraction, Zvyagin (1967) showed that dehydrated halloysite exhibits a higher degree of structural order than was previously inferred from XRD. Otherwise, halloysite tubes displaying lath-like morphology were considered by Churchman and Gilkes (1989) as kaolinite formed by prolonged dehydration of tubular halloysite, where dehydration of the hydrated 1:1 structure was explained by H bonding which became the dominant force favoring tetrahedral sheet rotation (Bailey, 1988).

The repulsive forces are usually due to the interaction between electrical double layers or from interaction between layers. Such repulsion forces may have caused a true mechanical fragmentation of kaolinite plates, producing lath-shaped kaolinite. Otherwise, un-

balanced forces (*i.e.* contraction of outer OH planes of the octahedral sheet or the unequal dimensions of the tetrahedral and octahedral sheets) may fracture the kaolinite plates that subsequently will curve/fold along a preferred crystallographic direction (Robertson and Eggleton, 1991; Singh and Gilkes, 1992).

Rolled/folded kaolinite plates constitute a unique genetic link between kaolinite and halloysite-7 Å, which confirms the transformation of kaolinite to halloysite-7 Å. A parallel orientation of the rolled/folded plates of kaolinite to a major crystallographic face is shown by TEM. This is in accord with Singh and Mackinnon (1996), who showed that the major crystallographic directions controlled the rolling-up of kaolinite plates.

Some defect layers represented by either deformations or layer terminations were identified locally by HRTEM in well-ordered kaolinite displaying a good crystallinity (HI = 1.07). It is assumed to be typical of kaolinite crystals, which supported a rapid growth. The geological environment associated with the shear zones facilitated a great discharge of metamorphic waters, generating large ion concentrations of solution and a rapid growth of kaolinite crystallite (Sunagawa, 1975).

The AEM data show no variation in the Si/Al ratio, of ~1 for both well-ordered kaolinite or rolled kaolinite plates. However, the ideal ratio of kaolinite is =1. During the passage from kaolinite to rolled kaolinite plates or folded lath-shaped kaolinite there is no clear evidence to support the hypothesis that the tetrahedral substitution took place along the transformation of kaolinite to halloysite-7 Å.

The FTIR spectra show changes in the resolution of the absorption bands corresponding to the Si–O–Si (including Si–O–Al) stretching region in the range 1100–950 cm^{-1}. The Si–O stretching bands show changes along the kaolinite to hallosyite-7 Å transition. Also, changes of vibrational bands were recorded in the FTIR spectrum of sample Hly-8 as a consequence of a reduced symmetry in kaolinite.

The ^{27}Al-MAS-NMR confirms a disorder in kaolinite structure arising as a result of Al-vacancy displacements in the octahedral sheet (Newman *et al.*, 1994). The three spectra of kaolinite samples have a similar shape and no major differences between the kaolinite spectrum and the halloysite spectrum could be detected.

The surface charge and electrophoretic properties of the kaolinite samples studied were discussed previously (Tari *et al.*, 1999). The cation exchange capacity increases slightly during the kaolinite to halloysite-7 Å transition, whereas the BET specific surface area retains almost the same value. Tari *et al.* (1999) combined the deprotonation effects of both siloxane and gibbsite sheets, reporting the effect of isomorphic substitution on the electrophoretic behaviour of the kaolinite to halloysite-7 Å transition. Some permanent negatively charged surface sites such as $(Al–O–Si)^-$ on the siloxane sheet will be induced by Al^{3+} for Si^{4+} substitution and promote electrostatic attraction of cations in order to ensure the electroneutrality of the system. According to Tari *et al.* (1999) the modification of charge density during the kaolinite to halloysite-7 Å transition was believed to be due to Al^{3+}-for-Si^{4+} isomorphous substitution. The same observation was made by other authors (McBride, 1976; Rand and Melton, 1976). Nevertheless, heterogeneous surface charge of kaolinite is well recognized. For instance, Grim (1967) shows that the surface negative charge of kaolinite is derived from broken bonds around the edges and from exposed basal hydroxyls. The pH values at ζ potential curve range from 3.5 to 5 for the three samples of kaolinite studied (Tari *et al.*, 1999), which is lower than is expected for a 1:1 structure. This shows that the basal hydroxyl surfaces behave as edges and are important charge surfaces (Ma and Eggleton, 1999).

Two mechanisms are suggested in literature: tetrahedral rotation for correction of the lateral misfit (Bailey, 1990) and reduction of interlayer cohesion due to Si–Si repulsion for correction of the same lateral misfit (Singh, 1996).

Bailey (1990) reinterpreted the Bates *et al.* (1950) model, assuming that in kaolinite there is tetrahedral rotation of the basal oxygens, whereas in halloysite the tetrahedral rotation is blocked by interlayer water adsorbed into holes between oxygen tetrahedra. Interlayer water may not have a real effect on tetrahedral rotation, but only to disrupt hydrogen bonding across the interlayer (Costanzo and Giese, 1985). Singh (1996) put forward a new model for halloysite rolling by which the misfit of the tetrahedral sheet is corrected by rolling instead of tetrahedral rotation in the hydrated 1:1 layers. The misfit is transmitted through Si–O bonds to Si planes and basal oxygen planes, being affected as a consequence of contraction of the apical oxygen plane. To correct the misfit between apical oxygen planes and the inner OH plane, either tetrahedral rotation or rolling of the 1:1 layer must have taken place. The most convenient way, shown by Singh (1996), is by rolling, which causes a minimum contraction of the Si and basal oxygen planes.

The big question derived from previous studies (Singh and Mackinnon 1996) is what causes hydration? The hydration of kaolinite surfaces can lead to the formation of different surface species such as Al–OH–Al groups at the gibbsite sheet, =AlOH and/or ≡SiOH groups at the edge surfaces and Si–O–Si groups at the siloxane sheet (Stumm, 1992). Changes on the edges and the exposed hydroxyl surfaces depend upon pH. Negative charges are developed at the edges according to the reaction: $Si–OH + OH^- = Si–O^- + H_2O$, when $[OH^-]$ concentrations increase (Ma

https://doi.org/10.1346/CCMN.2001.0490609 Published online by Cambridge University Press

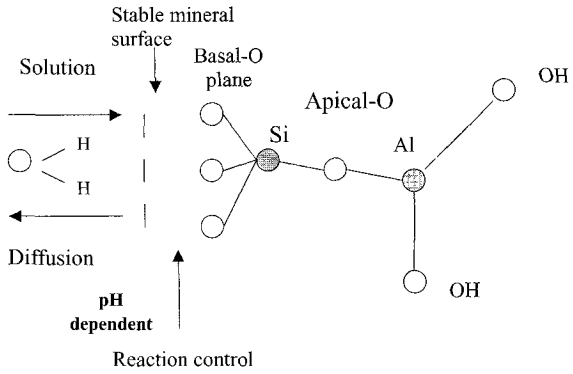

Figure 10. Schematic drawing of the siloxane sheet reacting with water. The reaction is through diffusion at the surface layer with solution.

and Eggleton, 1999). The same reaction may be applied to Al–OH at edges of an exposed basal surface. Otherwise, the Al^{3+} ion has a small ionic radius and a high electric charge, exercising a high polarization effect on water molecules.

Previous studies have considered that the transformation of kaolinite to halloysite-7 Å takes place in the solid state (Robertson and Eggleton, 1991; Singh and Gilkes, 1992). However, the solid-state transformation calls for ionic substitution of Al^{3+} for Si^{4+} within an intact silicate sheet and a planar kaolinite layer cannot roll after crystallization (Singh and Mackinnon, 1996). Therefore, it is likely that hydration of kaolinite produces a reaction at the mineral surface (Figure 10), which is rate controlled by the concentrations of the solutes. This reaction control is typically a detachment (desorption) or attachment (adsorption) of species (*i.e.* H_2O molecules) on the mineral surface. Exposure of the oxide surfaces to water causes the formation of surface OH groups (S–OH) that can be ionized. The pH of the medium influences the degree of ionization. At the particle/solution interface, the acid/base reactions occur resulting in surface charge development:

$$S\text{–}OH_2^+ \xleftarrow{H^+} S\text{–}OH \xrightarrow{OH^-} S\text{–}O^-$$

As the pH increases, deprotonation of the silica is continued, being more accentuated up to pH ≈ 6 and more gradual afterwards (Tari *et al.*, 1999). Therefore, the rate-determining step may be the diffusion through a solid layer at the siloxane sheet. This reaction type may contribute to the hydration of the kaolinite structure and subsequently the mechanism described by Singh (1996) should be a pathway of the kaolinite to halloysite-7 Å transformation.

CONCLUSIONS

The kaolinite samples selected from the same geological profile confirm the kaolinite to halloysite-7 Å transformation. The Hly-8 sample consists of a mixture of rolled kaolinite plates, and small and long tubes of halloysite-7 Å. The main conclusions are: (1) The kaolinite to halloysite-7 Å transition is accompanied by structural changes observed in both 02,1$\bar{1}$ and 1$\bar{3}$,13 reflections. (2) The FTIR spectra confirm structural changes during transition in the Si–O stretching band and Al–O–Si bending vibrations. The kaolinite hydration increases during kaolinite to halloysite-7Å transition. (3) The TEM data exhibit either thin kaolinite plates rolled/folded along a major crystallographic direction or folding of lath-shaped kaolinite. This is the unique genetic relationship between the two minerals. Well-ordered kaolinite contains some defect layers such as deformation or terminations, observed by HRTEM. (4) No tetrahedral substitution occurs during transition; (5) The surface OH group formation was ionized as a result of exposure of the oxide surface to water. The Si–O bonds are directed towards the contact points instead of lying normal to the basal plane and one of the basal oxygen atoms in each tetrahedron was raised above the other two and the siloxane surface becomes corrugated. The kaolinite structure in the near-surface water contact is modified towards a new structurally stable phase. The rate of reaction is a function of pH.

ACKNOWLEDGMENTS

I. Bobos gratefully acknowledges the Portuguese Foundation for Science and Technology for financial support (Praxis XXI BCC-4815), granted under his appointment as Invited Scientist. We are indebted to Associate Editor J. Elzea Kogel, to F. Elasass and to E. Galán for their constructive reviews and helpful comments. Thanks are due to A. Andrade and A.L. Lopes for their help with the XRD and TEM analyses.

REFERENCES

Anand, R.R., Gilkes, R.J., Armitage, T.M. and Hillyer, J.W. (1985) Feldspar weathering in a lateritic saprolite. *Clays and Clay Minerals,* **33,** 31–43.

Bailey, S.W. (1988) Polytypism of 1:1 layer silicates. Pp. 9–27 in: *Hydrous Phyllosilicates (exclusive of Micas)* (S.W. Bailey, editor). Reviews in Mineralogy, **19**. Mineralogical Society of America, Washington, D.C.

Bailey, S.W. (1990) Halloysite—a critical assessment. Pp. 89–98 in: *Proceedings of 9th International Clay Conference, Strasbourg* (V.C. Farmer and Y. Tardy, editors). Sciences Géologiques Mémoire, Strasbourg, France, **85**.

Banfield, J.F. and Eggleton, R.A. (1990) Analytical transmission electron microscope studies of plagioclase, muscovite and K-feldspar weathering. *Clays and Clay Minerals,* **38,** 77–89.

Bates, T.F., Hildebrand, F.A. and Swineford, A. (1950) Morphology and structure of endellite and halloysite. *American Mineralogist,* **6,** 237–248.

Bobos, I. and Gomes, C. (1998) Greisen and post-greisen alteration in the kaolin deposit of São Vicente de Pereira (Portugal). *Canadian Mineralogist,* **36,** 1621–1630.

Bobos, I. and Gomes, C. (1999) *Hydrothermal alteration and kaolinization in the north western border of Ossa Morena zone.* EUG 10, Abstract volume, **4.** Cambridge Publications, 592 pp.

Bobos, I. and Gomes, C. (2000) Dissolution of K-feldspar into Si-Al gel and crystallization of halloysite identified in

the kaolin deposit of São Vicente de Pereira (Portugal). *Geologica Carpathica,* **51,** 49–57.

Chaminé, H.I., Ribeiro, A. and Pereira, E. (1995) Cartografia geológica e estratigrafia da faixa precâmbrica do sector Espinho—Albergaria-A-Velha (Zona de Ossa-Morena). Faculdade de Ciências, Universidade do Porto. *Memória,* **4,** 329–333.

Churchman, G.J. and Gilkes, R.J. (1989) Recognition of intermediates in the possible transformation of halloysite to kaolinite in weathering profiles. *Clay Minerals,* **24,** 579–590.

Costanzo, P.M. and Giese, R.F. Jr. (1985) Dehydration of synthetic hydrated kaolinite: a model for the dehydration of halloysite (10 Å). *Clays and Clay Minerals,* **33,** 415–423.

Costanzo, P.M., Giese, R.F. Jr. and Clemency, C.V. (1984) Synthesis of a 10 Å hydrated kaolinite. *Clays and Clay Minerals*, **32,** 29–35.

Eswaran, H. and Bin, W.C. (1978) A study of deep weathering profile on granite in peninsular Malaysia: Mineralogy of the clay, silt and sand fractions. *Soil Science Society of America Journal,* **42,** 149–158.

Giese, R.F. Jr. (1988) Kaolin minerals: structures and stability. Pp. 29–66 in: *Hydrous Phyllosilicates (exclusive of Micas)* (S.W. Bailey, editor). Reveiws in Mineralogy, **19**. Mineralogical Society of America, Washington, D.C.

Gilkes, R.J., Anand, R.R. and Suddhiprakarn, A. (1986) How the microfabric of soils may be influenced by the structure and chemical composition of parent minerals. Pp. 1093–1106 in: *Trans International Soil Science Conference, Hamburg,* **6**.

Grim, R. (1967) *Clay Mineralogy.* McGraw Hill, New York, 596 pp.

Hinckley, D.N. (1963) Variability in "crystallinity" values among the kaolin deposits of the coastal plain of Georgia and South Carolina. *Clays and Clay Minerals,* **11,** 229–235.

Honjo, G., Kitamura, N. and Mihama, K. (1954) A study of clay minerals by means of single-crystal electron diffraction diagram—the structure of tubular kaolin. *Clay Minerals Bulletin,* **2,** 133–141.

Jackson, M.L. (1975) *Soil Chemical Analyses—Advanced Course.* Published by the author, Madison, Wisconsin, 895 pp.

Jiang, W.T. and Peacor, D.R. (1991) Transmission electron microscopic study of the kaolinisation of muscovite. *Clays and Clay Minerals,* **39,** 1–13.

Keller, W.D. (1978) Classification of kaolins exemplified by their textures in scanning electron microscopy. *Clays and Clay Minerals,* **26,** 1–20.

Kohyama, N., Fukushima, K. and Fukami, A. (1978) Observation of the hydrated form of tubular halloysite by an electron microscope equipped with an environmental cell. *Clays and Clay Minerals,* **26,** 25–40.

Ma, C. and Eggleton, R.A. (1999) Surface layer types of kaolinite: A high resolution transmission electron microscopy study. *Clays and Clay Minerals,* **47,** 181–191.

Ma, C., FitzGerald, J.D. Eggleton, R.A. and Llewellyn, D.J. (1998) Analytical electron microscopy in clays and other phyllosilicates: Loss of elements from a 90-nm stationary beam of 300 KeV electrons. *Clays and Clay Minerals,* **46,** 301–317.

MacEwan, D.M.C. and Wilson, M.J. (1980) Interlayer and intercalation complexes of clay minerals. Pp. 197–249 in: *Crystal Structures of Clay Minerals and Their X-ray identification* (G.W. Brindley and G. Brown, editors). Monograph **5**. Mineralogical Society, London.

McBride, M.B. (1976) A critique of diffuse double layer models applied to colloid and surface chemistry. *Clays and Clay Minerals,* **24,** 598–608.

Meunier, A. and Velde, B. (1979) Weathering mineral facies in altered granites: The importance of local small-scale equilibrium. *Mineralogical Magazine,* **43,** 261–268.

Newman, R.H., Childs, C.W. and Churchman, G.J. (1994) Aluminium co-ordination and structural disorder in halloysite and kaolinite by ^{27}Al NMR spectroscopy. *Clay Minerals,* **29,** 305–312.

Plançon, A. and Tchoubar, C. (1977) Determination of structural defects in phyllosillicates by X-ray powder diffraction. *Clays and Clay Minerals,* **25,** 436–450.

Plançon, A. and Zacharie, C. (1990) An expert system for the structural characterization of kaolinites. *Clay Minerals,* **25,** 249–260.

Plançon, A., Giese, R.F. and Snyder, R. (1988) The Hinckley index for kaolinites. *Clay Minerals,* **23,** 249–260.

Rand, B. and Melton, I.E. (1976) Particle interactions in aqueous kaolinite suspensions, I. Effect of pH and electrolyte upon the mode of particle interaction in homoionic sodium kaolinite suspensions. *Journal of Colloidal Interface Science,* **60,** 308–320.

Range, K.J., Range, A. and Weiss, A. (1969) Fire clay type kaolinite or fire clay minerals? Experimental classification of kaolinite-halloysite minerals. Pp. 3–13 in: *Proceedings International Clay Conference Tokyo, Volume 1.* (L. Heller and A. Weiss, editors). Israel University Press, Jerusalem.

Ribeiro, A., Pereira, E. and Severo, L. (1980) Análise da deformação da zona de cisalhamento Porto-Tomar na transversal de Oliveira de Azeméis. *Comunicação de Servicio Geologico de Portugal,* **66,** 3–9.

Robertson, I.D. and Eggleton, R.A. (1991) Weathering of granitic muscovite to kaolinite and halloysite and plagioclase-derived kaolinite to halloysite. *Clays and Clay Minerals*, **39,** 113–126.

Rocha, J. and Klinowski, J. (1990) ^{29}Si and ^{27}Al magic-angle-spinning NMR studies of the thermal transformation of kaolinite. *Physics and Chemistry of Minerals,* **17,** 179–186.

Rocha, J. and Pedrosa de Jesus, J.D. (1994) ^{27}Al satellite transition MAS NMR spectroscopy of kaolinite. *Clay Minerals,* **29,** 287–291.

Singh, B. (1996) Why does halloysite roll?—A new model. *Clays and Clay Minerals,* **44,** 191–197.

Singh, B. and Gilkes, R.J. (1992) An electron optical investigation of the alteration of kaolinite to halloysite. *Clays and Clay Minerals,* **40,** 212–229.

Singh, B. and Mackinnon, I. (1996) Experimental transformation of kaolinite to halloysite. *Clays and Clay Minerals,* **44,** 825–834.

Stoch, L. and Sikora, W. (1976) Transformation of micas in the process of kaolinization of granites and gneisses. *Clays and Clay Minerals,* **24,** 156–162.

Stumm, W. (1992) *Chemistry of the Solid-Water Interface.* Wiley & Sons, New York, 346 pp.

Sunagawa, I. (1975) Morphology of minerals. Pp. 509–587 in: *Morphology of Crystals* (I. Sunagawa, editor). Terra Science Publishes Co., Tokyo.

Tari, G., Bobos, I., Gomes, C. and Ferreira, J.M. (1999) Modification of charge density during the kaolinite to hallosyite-7 Å transformation. *Journal of Colloid Interface Surface,* **209,** 360–366.

Wada, K. (1961) Lattice expansion of kaolin minerals by treatment with potassium acetate. *American Mineralogist,* **46,** 78–91.

Wilke, B.S., Schwertmann, U. and Murad, E. (1978) An occurrence of polymorphic halloysite in granite saprolite of the Bayerischer Wald, Germany. *Clay Minerals,* **13,** 67–77.

Zvyagin, B.B. (1967) *Electron Diffraction Analysis of Clay Minerals Structures.* Plenum Press, New York, 364 pp.

E-mail of corresponding author: juliu@geo.ua.pt

(*Received 16 July 2000; revised 12 March 2001; Ms. 468; A.E. Jessica Elzea Kogel*)